# An Effective Medium Theory-Based Unified Model for Estimating Thermal Conductivity of Unfrozen and Frozen Soils

**Hailong Ji[1], Xue Fu[1], Zhuotong Nan[1,2], Shuping Zhao[1]**

[1]Key Laboratory of Ministry of Education on Virtual Geographic Environment, Nanjing Normal University, Nanjing, 210023, China

[2]Jiangsu Center for Collaborative Innovation in Geographical Information Resource Development and Application, Nanjing, 210023, China

Corresponding author: Zhuotong Nan (nanzt@njnu.edu.cn); Shuping Zhao (shuping@njnu.edu.cn)



Please cite as: Ji H, Fu X, Nan Z, Zhao S. An Effective Medium Theory-Based Unified Model for Estimating Thermal Conductivity in Unfrozen and Frozen Soils. Catena. 2024, 239: 107942. doi:10.1016/j.catena.2024.107942.

**Highlights:**

- A unified model was developed for unfrozen and frozen soil thermal conductivity
- New model accurately reproduces the increase at low moisture and during freezing
- High predicative scores were obtained using a large compiled dataset

**Abstract**

Soil thermal conductivity (STC) is a crucial parameter in modeling land surface processes. However, the current STC models are developed separately for unfrozen and frozen soils, leading to inconsistent understanding. In this study, we propose a unified model based on the work of Ghanbarian and Daigle (2016) originally developed for unfrozen soils. The unified model comprises three parameters: critical volume fraction ($\phi_c$), scaling exponent ($t$), and a compensating factor ($\alpha$), and considers dry soil as the low-conductivity component (weighted by air volume fraction) and saturated soil as the high-conductivity component (weighted by volumetric liquid content for unfrozen state and total water content for frozen state). Specifically, $\phi_c$ represents a critical point where high-conductivity component begins to govern the behavior of effective STC, characterized by $t$. $\alpha$ allows for accurate calibration of saturated STC. Using a dataset of 90 unfrozen samples (693 measurements) and 74 frozen samples (255 measurements), pedotransfer functions (PTFs) for the three parameters were trained. The unified model successfully reproduces the sharp rise in STC at low moisture conditions during wetting and the increase during freezing. Compared to an empirical model (Côté and Konrad, 2005a) and a theoretical model (Tian et al., 2016), the unified model demonstrates higher predictive skill for unfrozen and frozen soils, achieving Nash-Sutcliffe efficiency coefficients of 0.96 and 0.90, respectively. This work contributes to a more consistent and comprehensive understanding of STC in cold environments and has the potential to be integrated into land surface models.

**Keywords**

Soil thermal conductivity, Frozen soils, Effective medium approximation, Unified model, Pedotransfer function

# 1 Introduction

The Earth's changing thermal state has raised growing concerns, particularly in light of the recorded significant warming trends (Biskaborn et al., 2019) and the projected potential intensification (Zhang et al., 2022). Soil thermal conductivity (STC) plays a critical role in regulating thermal energy distribution, impacting physical (Burke et al., 2020; Ding et al., 2021), chemical (Colombo et al., 2018), and biological (Hu et al., 2022; Wang et al., 2023) processes at land surface and subsurface. Accurate and robust parameterization of STC is essential for advancing land surface models (LSMs) and achieving a comprehensive understanding of the tightly coupled interactions on the interface between land and atmosphere (Koven et al., 2013; Sun et al., 2023).

The intricacy of soil lies in its diverse composition including solid particles, air, liquid water, and ice. While the thermal conductivities of air (0.024 $Wm^{-1}°C^{-1}$), liquid water (0.56 $Wm^{-1}°C^{-1}$), and ice (2.22 $Wm^{-1}°C^{-1}$) are well-established, the thermal conductivity of solid particles varies between 1 and 5 $Wm^{-1}°C^{-1}$ depending on mineral compositions. However, accurately predicting STC becomes challenging when considering factors such as the ratio of each component (e.g., porosity, degree of saturation) (Chen, 2008; Smits et al., 2010), interactions between components (e.g., water film coating solid particles) (Lu and Dong, 2015), and the microstructure (e.g., contact among solid particles) (Farouki, 1981). Estimating STCs is relatively straightforward for completely dry and fully saturated states (He et al., 2021b; Wang et al., 2021), but it becomes more intricate for moist soils (Dong et al., 2015; Zhang and Wang, 2017) and partially frozen soils (He et al., 2021a).

Two main types of STC models have been developed: empirical and theoretical. Empirical models establish relationships between STC and influencing factors (e.g., texture, porosity, moisture

content) (Côté and Konrad, 2005a; Farouki, 1981; Johansen, 1975; Kersten, 1949; Peters-Lidard et al., 1998), providing a balance between accuracy and simplicity. Among them, the normalized concept, derived from Johansen (1975) and advanced by Côté and Konrad (2005a) (hereafter referred to as CK2005), has been widely used in LSMs (Dai et al., 2003; Niu et al., 2011; Wu et al., 2018).

On the other hand, theoretical models are based on idealized assumptions about the arrangement of components. Two well-known assumptions are series addition (i.e., arithmetic mean) and parallel addition (i.e., harmonic mean). The de Vries model (1963) assumes that solid particles are dispersed in a continuous fluid. This model has gained popularity and been extended to frozen soils by Farouki (1982). More recently, Tian et al. (2016) developed a simplified yet more general version by relating the shape factor to soil texture (hereafter referred to as Tian2016). Another noteworthy theoretical model, based on the General Effective Media (GEM) theory, was proposed by Ghanbarian and Daigle (2016) for unfrozen soils (hereafter referred to as GD2016) and had demonstrated advantage in depicting the sharp increase of STC caused by the effect of "liquid capillary bridge", which is essential to the form of continuous heat transfer pathways.

However, there still remains a lack of satisfactory STC model for frozen soils, of which the most are adaptions of those designed for frozen soils (Du et al., 2020; Li et al., 2019). The presence of ice complicates the heat conduction process in frozen soils, with ice having four times higher thermal conductivity and 0.92 times the density of liquid water. The phase change between ice and liquid water not only changes the volume ratio of soil components but also alters the contact area (Farouki, 1981), thereby affecting STC. Additionally, measuring STC under frozen state is prone to errors introduced by the latent heat absorbed during ice melting, especially at temperatures close to the freezing point (i.e., −4 to 0 °C) (Overduin et al., 2006; Tian et al., 2015). Though the transient

method is superior to the steady-state method, it still fails to avoid this flaw completely (Wan et al., 2022), resulting in relatively scarce and less precise measurements.

From the perspective of modeling, solving STCs separately for unfrozen and frozen states inevitably leads to jumping discontinuities around the phase change, causing inaccurate simulation results in LSM due to error propagation (Dai et al., 2019; Harp et al., 2016; Ren et al., 2023). The phase change is of great importance for studying cold-region land surface processes, such as the zero-curtain effect (Zhao et al., 2022) and active layer thickness (Smith et al., 2022; Zhao et al., 2010). A unified model that considers both unfrozen and frozen soils holds the potential to address these challenges. However, to the best of our knowledge, there are few unified models in this field, possibly due to the lack of an appropriate theoretical basis.

In this study, we propose a unified model applicable to both unfrozen and frozen conditions by extending the well-established GD2016 model. In Section 2, we present the unified model after reviewing the GD2016 model and provide details of the experimental design and measured dataset. Section 3 demonstrates the characteristics and capabilities of the unified model using measured data and the comparison with two selected models. Finally, we provide discussion in Section 4 and a concise summary of this study in Section 5.

# 2 Methods and Materials

## 2.1 The GD2016 model

The GD2016 model is rooted in the GEM equation proposed by McLachlan (1987, 1986, 1985), which combines the effective medium approximation to constrain the lower and higher bounds and the percolation theory to refine the transition behavior near the critical regime. Ghanbarian and Daigle (2016) adapted the GEM equation for STC ($\lambda_{eff}$) in unfrozen conditions by designating

complete dry soil (with STC represented by $\lambda_{dry}$) as the low-conductivity component (LCC) and fully saturated soil (with STC represented by $\lambda_{sat}$) as the high-conductivity component (HCC). The GD2016 model is expressed in Equation (1):

$$\left(n-\theta_{liq}\right)\frac{\lambda_{dry}^{1/t}-\lambda_{eff}^{1/t}}{\lambda_{dry}^{1/t}+\left(\frac{n-\phi_c}{\phi_c}\right)\lambda_{eff}^{1/t}}+\theta_{liq}\frac{\lambda_{sat}^{1/t}-\lambda_{eff}^{1/t}}{\lambda_{sat}^{1/t}+\left(\frac{n-\phi_c}{\phi_c}\right)\lambda_{eff}^{1/t}}=0 \tag{1}$$

where the volume fraction of air ($n-\theta_{liq}$) and liquid water ($\theta_{liq}$) in the soil pores determines the weighting of the LCC and HCC, respectively. $n$ is the soil porosity. The parameter $\phi_c$, referred to as critical volume fraction, represents the point at which $\lambda_{eff}$ transitions from $\lambda_{dry}$ to $\lambda_{sat}$, analogous to the percolation threshold in percolation theory. As $\theta_{liq}$ increases to $\phi_c$, a continuous cluster, akin to a heat transfer path for thermal conduction, forms across the material, leading to $\lambda_{eff}$ dominated by $\lambda_{sat}$. Conversely, for smaller $\theta_{liq}$, the clusters become finite and isolated (Kirkpatrick, 1973), which indicates that $\lambda_{eff}$ is closer to $\lambda_{dry}$. The scaling exponent, $t$, inherited from the GEM equation, characterizes the transitional behavior of the transport property around $\phi_c$ to accommodate non-spherical shapes of the components, such as (randomly) oriented ellipsoids (McLachlan, 1987).

Using a dataset of 17 unfrozen soil samples, Sadeghi et al. (2018) derived soil pedotransfer functions (PTFs) for the model parameters $\phi_c$ and $t$:

$$\phi_c = 0.33 f_{clay} \tag{2}$$

$$t = -0.25 f_{clay} + 0.342 \tag{3}$$

where $f_{clay}$ denotes the fraction of clay. However, $\lambda_{dry}$ and $\lambda_{sat}$ were treated as tunning parameters without explicit PTFs.

## 2.2 The unified model

We propose a unified STC model by extending the GD2016 model to cover both unfrozen soils and frozen soils:

$$\left(n-\theta_{liq}-\theta_{ice}\right)\frac{\lambda_{dry}^{1/t}-\lambda_{eff}^{1/t}}{\lambda_{dry}^{1/t}+\left(\frac{n-\phi_c}{\phi_c}\right)\lambda_{eff}^{1/t}}+\left(\theta_{liq}+\theta_{ice}\right)\frac{\left(\alpha\lambda_{sat}\right)^{1/t}-\lambda_{eff}^{1/t}}{\left(\alpha\lambda_{sat}\right)^{1/t}+\left(\frac{n-\phi_c}{\phi_c}\right)\lambda_{eff}^{1/t}}=0 \quad (4)$$

where the sum of liquid and ice contents ($\theta_{liq}+\theta_{ice}$), also known as total water content, determines the weight of HCC. A compensating factor, $\alpha$, is newly introduced to mitigate uncertainty in estimating $\lambda_{sat}$ (Equation (6)–(8)). When $\theta_{ice}=0$ and $\alpha=1$, the unified model reduces to GD2016 for unfrozen soils. $\lambda_{sat}$ for frozen soils represents the STC in saturation but under extreme naturally cold conditions (assumed to be −40 °C in this study), while for unfrozen soils, $\lambda_{sat}$ remains independent of soil temperature.

To estimate $\lambda_{dry}$, we adopt the empirical relation developed by Côté and Konrad (2005a) for its high accuracy:

$$\lambda_{dry}=\chi 10^{-\eta n} \quad (5)$$

where $\chi$ and $\eta$ are empirical parameters. $\chi$ equals 1.70 for gravels, 0.75 for natural mineral soils, and 0.30 for peat, while $\eta$ is assigned the values 1.80, 1.20, 0.87, respectively. $\lambda_{sat}$ is estimated using a geometric mean (Côté and Konrad, 2005a):

$$\lambda_{sat}=\lambda_{solid}^{1-n}\lambda_{liq}^{\theta_{liq,sat}}\lambda_{ice}^{1.09(n-\theta_{liq,sat})} \quad (6)$$

where $\theta_{liq,sat}$ represents the saturated liquid water content. For unfrozen soils, $\theta_{liq,sat}$ is equal to the porosity $n$, so eliminating the term $\lambda_{ice}$. For frozen soils, $\theta_{liq,sat}$ is calculated as the maximum

unfrozen water content at −40°C, as explained in Section 2.3. The term $1.09(n-\theta_{liq,sat})$ represents the ice fraction considering the density difference. $\lambda_{solid}$ is the thermal conductivity of solid particles, depending on the forming minerals, which can vary from 2 $Wm^{-1}°C^{-1}$ (e.g., plagioclase) to 8 $Wm^{-1}°C^{-1}$ (e.g., silica) (Horai, 1971). Given often unavailability of mineral contents in measurements, we estimate $\lambda_{solid}$ using quartz content, $f_{quartz}$ (Johansen, 1975), which is approximately a function of sand content, $f_{sand}$ (He et al., 2021a), when quartz information is absent in soils:

$$\lambda_{solid} = \lambda_{quartz}^{f_{quartz}} \lambda_{others}^{1-f_{quartz}} \tag{7}$$

$$f_{quartz} = 0.5 f_{sand} \tag{8}$$

where $\lambda_{others}$ for any other forming minerals is assigned a value of 2 $Wm^{-1}°C^{-1}$ when $f_{quartz}$ > 0.2, otherwise, 3 $Wm^{-1}°C^{-1}$, while $\lambda_{quartz}$ is a constant value of 7.7 $Wm^{-1}°C^{-1}$.

### 2.3 Estimation of unfrozen water content in frozen soils

In Equations (4) and (6), $\theta_{liq}$ and $\theta_{liq,sat}$ for frozen soils are related to soil temperature. One commonly used method for estimating $\theta_{liq}$ for frozen soils involves using soil water potential ($\Psi$) as an intermediary, connecting $\theta_{liq}$ and soil temperature, $T$. The relation between $\Psi$ and $\theta_{liq}$ was given by Brooks (1965):

$$\psi = A\theta_{liq}^{B} \tag{9}$$

where $A$ and $B$ are parameters related to soil texture, with values provided by Saxton et al. (1986):

$$A = \exp\left(-4.396 - 7.15 f_{clay} - 4.880 f_{sand}^{2} - 4.285 f_{sand}^{2} f_{clay}\right) \times 100 \tag{10}$$

$$B = -3.140 - 22.2 f_{clay}{}^{2} - 3.484 f_{sand}^{2} f_{clay} \tag{11}$$

where the constant 100 is used to convert from the unit of bar to kPa.

Meanwhile, the Clausius-Clapeyron equation describes the relation between $\Psi$ and $T$, with a simplified version applicable to frozen soils (Kurylyk and Watanabe, 2013):

$$\psi = \frac{L_f \rho_{liq}}{1000}\left(\frac{T}{273.15}\right) \tag{12}$$

where $\rho_{liq}$ denotes liquid water density (1000 kg m$^{-3}$), $L_f$ is the latent heat of fusion (3.34 ×10$^5$ J kg$^{-1}$), 1000 is the conversion factor from Pa to kPa. By combining Equations (9) and (12), the maximum unfrozen water content, $\theta_{uwc,max}$, can be estimated from $T$ as follows:

$$\theta_{uwc,max}(T) = \left|\frac{\psi}{A}\right|^{1/B} \tag{13}$$

$\theta_{uwc,max}(T)$ represents the theoretically maximum unfrozen water content at a given sub-zero temperature and can be used to estimate $\theta_{liq}$, as shown in Equation (14).

$$\theta_{liq} = \min\left(\theta_{ini}, \theta_{uwc,max}(T)\right) \tag{14}$$

where $\theta_{ini}$ is the initial water content before the onset of freezing. For a given temperature, $T < 0$ °C, when $\theta_{ini}$ exceeds $\theta_{uwc,max}(T)$, $\theta_{liq}$ takes $\theta_{uwc,max}(T)$, and the excess part will undergo a phase change to ice. Obviously, $\theta_{liq,sat}$ for frozen soils equals $\theta_{uwc,max}$ (−40°C) in our setting.

## 2.4 Measured dataset

In this study, we complied a dataset consisting of 90 unfrozen soil samples totaling 693 measurements, and 74 frozen soil samples totaling 255 measurements, from published literature. Each soil sample in the dataset corresponds to consistent soil texture and dry bulk density ($\rho_d$) to account for variations that impact STC. A measurement is a unique combination of STC and total

water content for a soil sample. We followed the criteria set by He et al. (2021a) for filtering the measurements. These criteria include: (1) using reliable and reproducible experimental technique/setup, with $\lambda_{eff}$ measured using either the transient heat pulse or steady-state method; (2) having detailed descriptions of specimen preparation and complete information on soil texture, porosity, dry bulk density; and (3) providing a sufficient number of measurements per sample. The essential details of the collected samples are presented in **Table 1**, with the corresponding distribution of soil texture depicted in **Figure 1**.

**Table 1** Basic information of unfrozen and frozen samples used in this study.

| State | Source | Sand | Silt | Clay | Temp.[1] | $\rho_d$ [2] | $n$ [3] | $\theta_{tot}$ [4] | # of samples[5] | # of meas. | Method[6] |
|---|---|---|---|---|---|---|---|---|---|---|---|
| | | | | | (°C) | (kg m$^{-3}$) | (m$^3$ m$^{-3}$) | (m$^3$ m$^{-3}$) | | | |
| Unfrozen | McInnes (1981) | 0.20 – 0.95 | 0.03 – 0.68 | 0.02 – 0.24 | … | 1251 – 1500 | 0.43–0.53 | 0 – 0.33 | 5 | 76 | Transient method (TCP) |
| | Campbell et al. (1994) | 0.09 – 0.89 | 0.06 – 0.70 | 0.05 – 0.47 | … | 760 – 1500 | 0.43 – 0.71 | 0 – 0.39 | 9 | 85 | Transient method (TCP) |
| | Kasubuchi et al. (2007) | 0.28 – 1.00 | 0 – 0.58 | 0 – 0.43 | … | 854 – 1620 | 0.40 – 0.65 | 0 – 0.65 | 4 | 43 | Transient method (TCP) |
| | Lu et al. (2007) | 0.08 – 0.94 | 0.01 – 0.70 | 0.05 – 0.32 | … | 1293 – 1600 | 0.41 – 0.52 | 0 – 0.52 | 10 | 121 | Transient method (Thermo-TDR) |
| | Chen (2008) | 0.17 – 0.94 | 0.06 – 0.59 | 0 – 0.24 | … | 1201 –1712 | 0.35 – 0.55 | 0 – 0.55 | 16 | 80 | Transient method (TCP) |
| | Tarnawski and Leong (2012) | 1 | 0 | 0 | … | 1590 –1802 | 0.32 – 0.40 | 0 – 0.4 | 6 | 48 | Transient method (TCP) |
| | Tarnawski et al. (2015) | 0 – 1 | 0 – 0.83 | 0 – 0.42 | … | 976 – 1708 | 0.36 – 0.63 | 0 – 0.63 | 40 | 240 | Transient method (TCP) |
| Frozen | Kersten (1949) | 0.08 – 1 | 0 – 0.81 | 0 – 0.27 | −30 – 5 | 1277 – 2020 | 0.25 – 0.53 | 0.19 – 0.38 | 20 | 70 | Steady-state method |
| | Penner et al. (1975) | 0 – 0.9 | 0 – 0.71 | 0.04 – 0.56 | −25 – 5 | 1491 – 1970 | 0.28 – 0.46 | 0.07 – 0.33 | 19 | 45 | Transient method (Heat flow) |
| | Tian et al. (2016) | 0.07 – 0.94 | 0.01 – 0.60 | 0.01 – 0.43 | −10 | 1209 – 1585 | 0.40 – 0.54 | 0.08 – 0.36 | 19 | 20 | Transient method (Thermo-TDR) |
| | Zhang et al. (2018) | 0.39 | 0.54 | 0.07 | −19 – 8 | 1500 | 0.43 | 0.19 – 0.30 | 4 | 36 | Transient method (SPHP) |
| | Lu et al. (2018) | 0.88 | 0.12 | 0 | −15 – 1 | 1600 | 0.40 | 0.11 – 0.24 | 3 | 15 | Transient method (SPHP) |
| | Kojima et al. (2018) | 0.50 | 0.29 | 0.21 | −15 – 1 | 1200 | 0.56 | 0.16 – 0.46 | 4 | 24 | Transient method (DPHP) |
| | Xu et al. (2020) | 0.18 | 0.45 | 0.37 | −38 – 6 | 1650 – 1830 | 0.33 – 0.39 | 0.27 – 0.35 | 5 | 45 | Transient method (Line heat) |

[1] Unfrozen samples were measured under room temperature ranging from 4 to 25 °C;
[2] $\rho_d$, dry bulk density;
[3] $n$, porosity;
[4] $\theta_{tot}$, total water content (liquid + ice fraction);
[5] A soil sample corresponds to consistent soil texture and dry bulk density;
[6] TCP: thermal conductivity probe; TDR: time-domain reflectometry; SPHP: single probe heat pulse; DPHP: dual probes heat pulse.

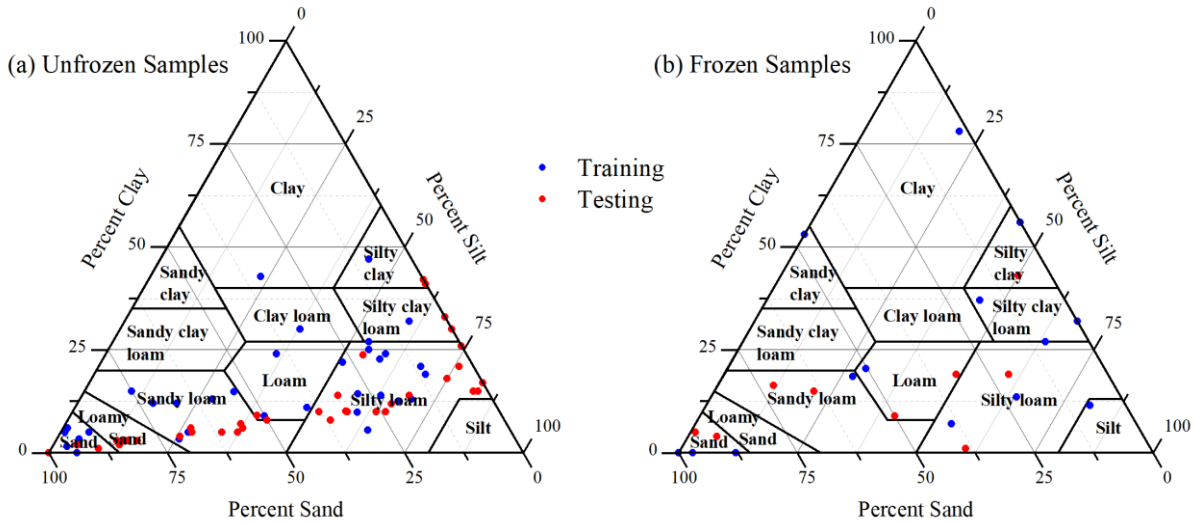


**Figure 1** Distribution of soil samples over particle size triangles for (a) unfrozen and (b) frozen soils. The training and testing samples are presented separately by blue and red dots, respectively.

## 2.5 Experiment design

The unified model fits each sample by optimizing the model parameters: the critical volume fraction ($\phi_c$), scaling exponent ($t$), and compensating factor ($\alpha$) to minimize the objective function. To ensure realistic parametric values, the effective ranges of the parameters are set as follows: [0.0, $n$] for $\phi_c$, [0.0, 0.6] for $t$, and [0.5, 1.5] for $\alpha$, based on previous studies (Ghanbarian and Daigle, 2016; McLachlan et al., 1990; Sadeghi et al., 2018) and expert knowledge. The upper limit of $\phi_c$ is constrained not to exceed porosity, $n$, which also acts as the maximum HCC fraction. The range of $t$ is slightly expanded from the range of [0.2, 0.4] suggested by Ghanbarian and Daigle (2016) to account for potential shifts in the saturation-dependent curve for frozen soils. The range of α is limited to [0.5, 1.5] to balance the flexibility in correcting $\lambda_{sat}$ estimation and the risk of over-fitting, which could yield inappropriate results for $\phi_c$ and $t$. Parameter fitting uses a particle swarm optimization R package (Claus, 2022).

To establish the PTFs for the model parameters and validate the new model, the compiled dataset was divided into two independent datasets: one for training (about 2/3 of total measurements) and the other for testing (remaining 1/3) (**Figure 1**). However, considering the uneven distribution of soil texture in the samples and to ensure independent validation from calibration, we opted for purposeful division over random division. Specifically, for unfrozen soils, the measurements from Tarnawski et al. (2015) were used as the testing set (40 samples, 240 measurements), while for frozen soils, the measurements of Penner (1975) and Tian et al. (2016) were used as the testing set (38 samples, 65 measurements). The remaining samples were used as the training set.

Using the training dataset, strongly explanatory variables were identified based on pairwise correlation coefficients between the fitted model parameters and soil properties. PTFs were then established using simple linear regression after removing some outliers. For parameters that did not show a strong correlation with the soil properties, the median value was used as a substitute to ensure generality. Upon the establishment of the PTFs, the new model was applied to estimate STCs for samples in the testing set.

We chose the CK2005 and Tian2016 models as reference models for comparison, with the detailed description provided in Section 2.6. These models were individually optimized to explore their best potential performance (Section 3.1), while their default PTFs were used for evaluating the capability to predict the testing dataset (Section 3.4), resembling a real-world scenario used in an LSM. Additionally, the GD2016 model was also included in the comparative analysis for unfrozen samples.

Three metrics were used to assess the model performance: bias, root-mean-square error (RMSE), and Nash-Sutcliffe efficiency (NSE):

$$bias = \frac{1}{N}\sum_{i=1}^{N}\left(P_i - O_i\right) \tag{15}$$

$$RMSE = \sqrt{\frac{1}{N}\sum_{i=1}^{N}\left(P_i - O_i\right)^2} \tag{16}$$

$$NSE = 1 - \frac{\sum_{i=1}^{N}\left(P_i - O_i\right)^2}{\sum_{i=1}^{N}\left(O_i - \bar{O}\right)^2} \tag{17}$$

where $N$ is the total number of measurements; $\bar{O}$ is the mean of measurements ($O_i$); $P_i$ is the predicted value. Bias indicates the absolute error, with positive values indicating overestimation by the model and negative values indicating underestimation. RMSE complements bias by considering the squared errors, which is also used as the objective function in parameter optimization. NSE quantifies the predictive skill in terms of the variance with reference to the mean of measurements, ranging from $-\infty$ to 1. An NSE value of 0 indicates the same prediction as the mean, while an NSE value of 1 represents a perfect prediction where the error variance is zero.

## 2.6 Two compared models

Three criteria guided the selection of reference models: (1) widespread use with high-accuracy estimates; (2) representation of either empirical or theoretical types; (3) capability to model STC for both unfrozen and frozen soils. Ultimately, the CK2005 and Tian2016 models were chosen as representatives of empirical and theoretical models, respectively.

### 2.6.1 CK2005: An empirical model based on the normalized concept

Johansen (1975) proposed a concept of normalized STC:

$$\lambda_{eff} = k_r\left(\lambda_{sat} - \lambda_{dry}\right) + \lambda_{dry} \tag{18}$$

where $k_r$ is the Kersten number. Côté and Konrad (2005a) advanced the model by offering a scheme for dry and saturated soils as well as $k_r$:

$$k_r = \frac{\kappa S_r}{1+(\kappa-1)S_r} \tag{19}$$

where $S_r$ denotes the degree of saturation, and $\kappa$ is an empirical parameter to account for the variability in soil types and the frozen/unfrozen state. For unfrozen (frozen) soils, the value for $\kappa$ is 4.60 (1.70) for gravels and coarse sands, 3.55 (0.95) for medium and fine sands, 1.90 (0.85) for silty and clayey soils, and 0.60 (0.25) for peat. In our experiment, we calibrated the value of $\kappa$ for each soil sample to explore its best potential in fitting the measurements. The same methods for estimating $\lambda_{sat}$ and $\lambda_{dry}$ have been incorporated into the unified model as Equations (5) to (7).

2.6.2 Tian2016: A theoretical model based on de Vries model

The de Vries model represents the thermal conductivity as a sum of contributions from each component (Farouki, 1982):

$$\lambda_{eff} = \frac{\sum_{j=0}^{N} k_j f_j \lambda_j}{\sum_{j=0}^{N} k_j f_j} \tag{20}$$

where $\lambda_j$ denotes thermal conductivity, $k_j$ the normalized thermal gradient, and $f_j$ the volume fraction for component $j$ in a medium with a total of $N+1$ components (i.e., solid, air, liquid water and ice). Specifically, the 0-th component is the continuous medium, which is the air in completely dry soil or water in moist soil. Other component, detonated by $j$ (where $1 \leq j \leq N$), is assumed as a rotational ellipsoid (i.e., an ellipsoid with two equal semi-diameters). Assuming heat flux parallel to the rotational axis, $k_j$ can be expressed as follows:

$$k_j = \frac{2}{3}\left[1+\left(\frac{\lambda_j}{\lambda_0}-1\right)g_{a(j)}\right]^{-1} + \frac{1}{3}\left[1+\left(\frac{\lambda_j}{\lambda_0}-1\right)\left(1-2g_{a(j)}\right)\right]^{-1} \tag{21}$$

where $g_a$ is the shape factor of $j$-th component, whose value equals the demagnetization coefficient.

Tian et al. (2016) improved the de Vries model in various aspects. First, the thermal conductivity and shape factor of solid particles were estimated based on the soil texture:

$$\lambda_{solid} = \lambda_{sand}^{f_{sand}} \lambda_{silt}^{f_{silt}} \lambda_{clay}^{f_{clay}} \tag{22}$$

where $\lambda_{sand}$ = 7.7 Wm$^{-1}$°C$^{-1}$, $\lambda_{silt}$ = 2.74 Wm$^{-1}$°C$^{-1}$, $\lambda_{clay}$ = 1.93 Wm$^{-1}$°C$^{-1}$, and

$$g_{a(solid)} = g_{a(sand)} f_{sand} + g_{a(silt)} f_{silt} + g_{a(clay)} f_{clay} \tag{23}$$

where $g_{a(sand)}$ = 0.182, $g_{a(silt)}$ = 0.0534, $g_{a(clay)}$ = 0.00775. Second, the shape factor of air and ice were related to their volume fractions ($f$) relative to the porosity ($n$), which characterizes the hypothetical ellipsoids from the needle prolate spheroid ($g_a$ = 0) to the sphere ($g_a$ = 1/3).

$$g_{a(air)} = \frac{1}{3}\left(1 - \frac{f_{air}}{n}\right) \tag{24}$$

$$g_{a(ice)} = \frac{1}{3}\left(1 - \frac{\theta_{ice}}{n}\right) \tag{25}$$

Third, the effect of vapor on thermal conductivity was ignored due to its minor role in modern transient measurements. Additionally, the de Vries-based model required a multiplier of 1.25 to adjust for the case of completely dry soils. To align with Tian et al. (2016), who established PTFs for $\lambda_{silt}$ and $g_{a(silt)}$, we also calibrated the same two parameters for the Tian2016 model.

# 3 Results

## 3.1 Reproduction of STC characteristics across wetting and freezing processes

**Figure 2** illustrates the performance of the models in reproducing STC changes during the wetting and freezing processes across various soil textures, ranging from fine particles (clay) to coarse particles (sand). For unfrozen soils, the unified model effectively reproduces the rapid increase in STC at the critical water content ($\phi_c$), as well as the gentle changes at low and high liquid water content (**Figure 2**a–c), with an average bias of −0.01 $Wm^{-1}°C^{-1}$, an NSE of 0.99, and all RMSE values below 0.05 $m^3m^{-3}$. As the solid particles change from fine-grained to coarse-grained, $\phi_c$ decreases from 0.15 to 0.01 $m^3m^{-3}$. This reduction is due to the fact that $\phi_c$ characterizes the formation of a "liquid capillary bridge" between solid particles, which requires more water to form in fine-grained soil due to its larger specific surface area (Anderson and Tice, 1972; Chen, 2008). Upon the formation of "liquid capillary bridge", the contribution to STC of replacing air with water is limited, resulting in the observed gentle changes. Despite the lack of the compensating factor α, the GD2016 model can still capture the changes in STC, but at the cost of using $\lambda_{dry}$ and $\lambda_{sat}$ as adjustable parameters.

In contrast, the CK2005 and Tian2016 models predict an increase in STC during the wetting process, but with a logarithmic curve shape, starting with a constant value of 0 $m^3m^{-3}$. This leads to an overestimation of STC for fine-grained soils when the soil moisture content is low (NSE ≤ 0.88). In addition, for the selected coarse soil sample (**Figure 2**c), they consistently underestimate the measured STCs (bias ≤ −0.24 $Wm^{-1}°C^{-1}$) except for the completely dry condition.

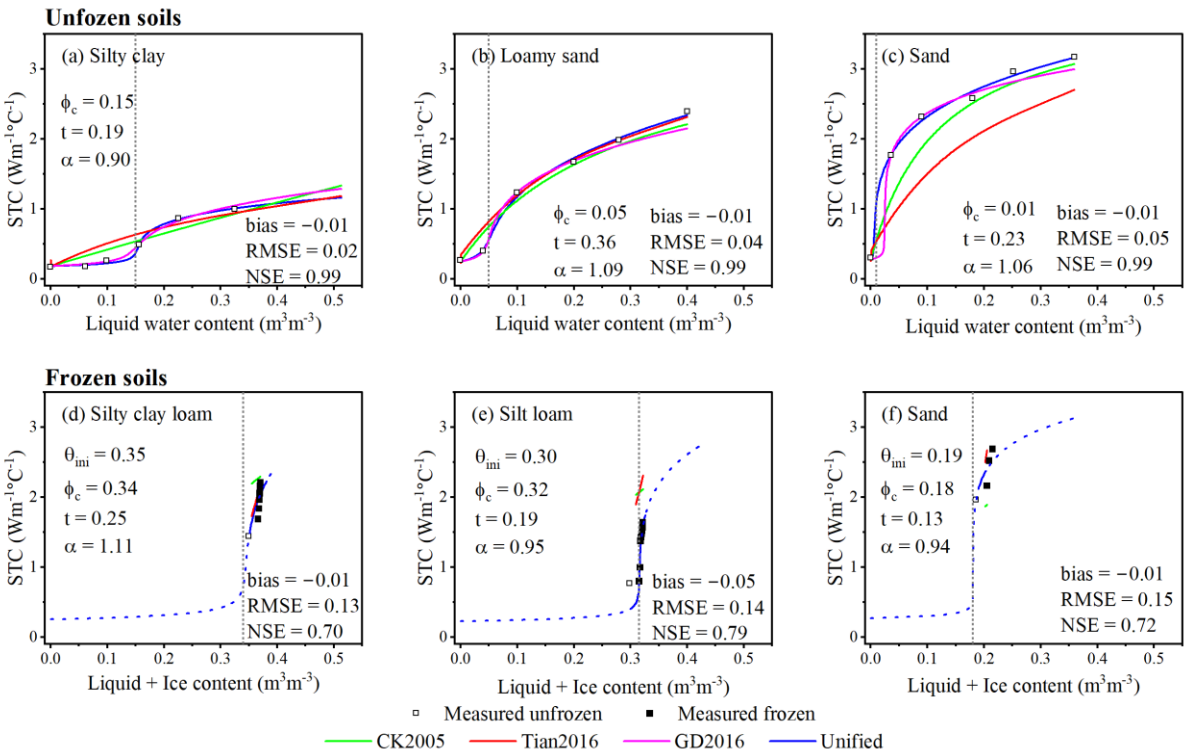


**Figure 2** Simulated soil thermal conductivity (STC) as a function of water content for selected unfrozen (a–c) and frozen (d–f) soil samples using different STC models. Hollow squares represent measurements under unfrozen state, while black solids for frozen state. The colored solid curves represent the simulation results of the models. Dashed blue lines represent values beyond the meaningful domain of the unified model (from $\theta_{ini}$ to $1.09\theta_{ini} - 0.09\theta_{uwc,max}(-40°\mathrm{C})$ given ice dilation). The dotted vertical line indicates the critical volume fraction ($\phi_c$) of the unified model. The values of the three parameters as well as initial water contents ($\theta_{ini}$), along with the performance metrics of the unified model are labeled. Note that GD2016 is only applicable to unfrozen soils. The measurements of (a) were from Lu et al. (2014), (b) and (c) from Tarnawski et al. (2015), (d) from Xu et al. (2020), (e) from Zhang et al. (2018), and (f) from Kersten (1949).

Compared to the other two models, the unified model provides more reliable simulations of the changes in STC caused by freezing (**Figure 2**d–f). For the fine-grained silt clay loam sample

(**Figure 2**d), both the Tian2016 and unified models perform well (bias ≤ 0.14 $Wm^{-1}°C^{-1}$, RMSE ≤ 0.19 $Wm^{-1}°C^{-1}$), while CK2005 tends to overestimate it (bias = 0.32 $Wm^{-1}°C^{-1}$, RMSE = 0.38 $Wm^{-1}°C^{-1}$). In the case of the silty loam sample (**Figure 2**e), both the Tian2016 and CK2005 models predict overestimated values (bias ≥ 0.80 $Wm^{-1}°C^{-1}$), while the unified model perfectly reproduces the changes in STC (bias = −0.05 $Wm^{-1}°C^{-1}$). Regarding the coarse-grained sand sample (**Figure 2**f), Tian2016 overestimates the STC (bias = 0.28 $Wm^{-1}°C^{-1}$), and CK2005 underestimates the STC (bias = −0.45 $Wm^{-1}°C^{-1}$). In contrast, the unified model provides a moderate prediction that appears to be closer to the mean STC measurements in magnitude (bias = −0.01 $Wm^{-1}°C^{-1}$). CK2005 exhibits poor performance for the frozen soil samples (NSE < 0) and tends to predict a constant value under varying negative temperatures. This may be attributed to the insensitivity of the Kersten number to changes in saturation during freezing.

**Figure 3** offers a different perspective on the changes in STC along with decreasing temperature, but based on the same simulated results as shown in **Figure 2**d–f. The unified model effectively captures the trend of a rapid increase at the early freezing stage, which is particularly evident in the silt loam sample (**Figure 3**b). Tian2016 and CK2005 show similar abilities in representing the rapid increase at the beginning of freezing but with substantial biases. For the coarse-grained sand sample, all three models fail to capture the gradually increasing pattern observed in the measurements (**Figure 3**c). Nevertheless, the unified model more accurately approximates the magnitude of measured STCs, indicating its better performance in this aspect. Meanwhile, the amplitudes of STC variations predicted by all three models appear smaller than those of the measured data, possibly due to challenges in estimating unfrozen water content in the frozen state.

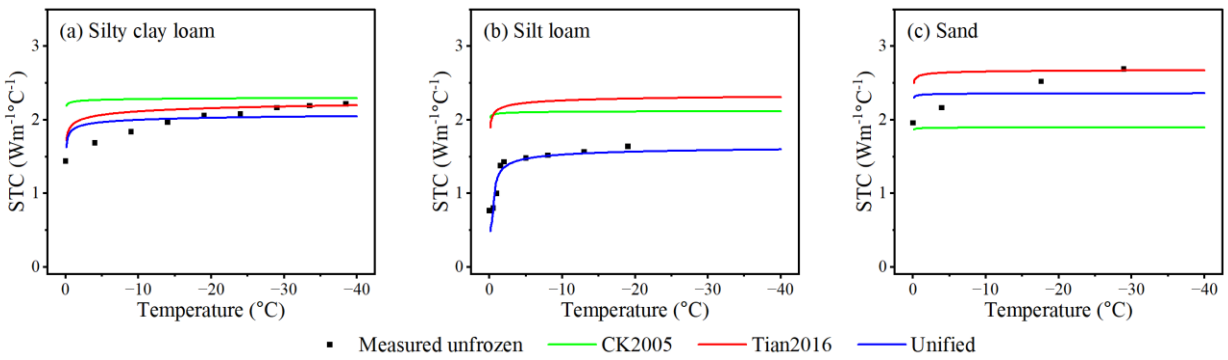


**Figure 3** Simulated STC as a function of freezing temperature. The data are the same as **Figure 2**d–f.

### 3.2 Unification of STC behaviors

To further demonstrate the capability of the new proposed model for a unified representation of STC for both unfrozen and frozen states, additional simulations were conducted on a silt loam sample (Zhang et al., 2018). **Figure 4** shows the simulated STC variations in both wetting and freezing processes. Associated fitted parameter values and performance metrics are provided in **Table 2**. The simulations reveal a smooth transition between unfrozen and frozen STC, even with small gaps present. For a given soil sample, the unified model effectively predicts STC at any liquid content, illustrated by the blue line in **Figure 4**, as the soil becomes wetter. At a certain $\theta_{ini}$, once the soil begins to freeze, the STC rapidly increases along the upward lines in **Figure 4**. In the unified model, the sum of liquid and ice contents is considered as the volume fraction of HCC (Equation (4)), which increases during freezing due to ice dilation. Hence, the simulation results are meaningful within a specific domain spanning from $\theta_{ini}$ to $1.09\theta_{ini} - 0.09\theta_{uwc,max}(-40°\mathrm{C})$, as depicted by solid lines in **Figures** 2 and 4. As a result, the model unifies and describes both the wetting process in unfrozen soils and the freezing process in frozen soils, a feature not commonly observed in existing STC models. Typically, separate models in different mathematical forms are

selected to simulate STC for unfrozen and frozen soils, often leading to gaps that occur when transitioning from unfrozen to frozen states. The unified approach ensures a seamless representation of STC behavior across wetting and freezing processes.

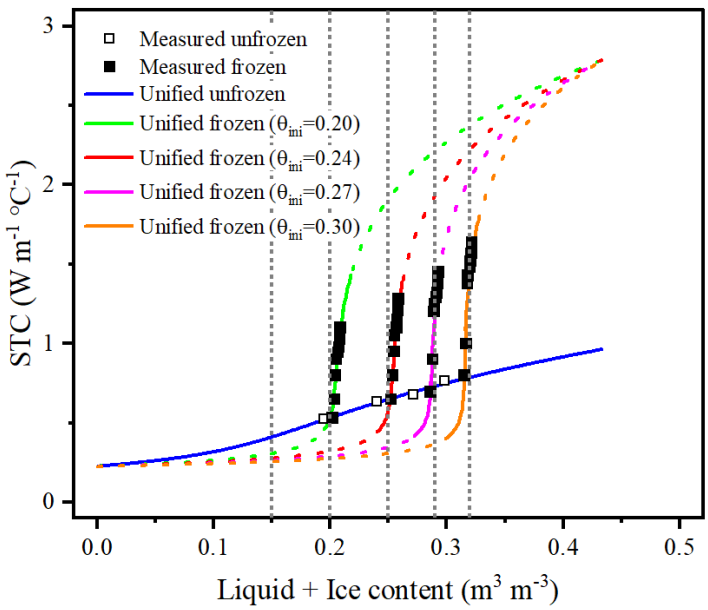


**Figure 4** Variations in thermal conductivity during both wetting and freezing processes as a function of total water content for a silt loam sample. The "unified unfrozen" experiment resembles a wetting process, while the others represent freezing processes with varying $\theta_{ini}$. The abscissa represents total water content (liquid water content in unfrozen state, and the sum of liquid and ice contents in frozen state). Hollow squares denote measurements under unfrozen state, while black solid squares represent measurements under frozen state. Dashed blue lines indicate values beyond the meaningful domain of the unified model. Dashed vertical lines indicate the fitting values of $\phi_c$ for the five experiments. The measured data are sourced from Zhang et al. (2018).

The impact of $\theta_{ini}$ on model performance (**Table 2**) is evident, as manifested by the underestimation of STC during the early freezing stage (i.e., the abscissa close to $\theta_{ini}$ in **Figure 4**). This discrepancy may be attributed to the underestimated $\theta_{uwc,max}$, where the impact is minor

when $\theta_{ini}$ is small but becomes more pronounced with larger $\theta_{ini}$ , resulting in a significant overestimation of $\theta_{ice}$ (Equation (14)). To mitigate this bias in future applications, one potential solution is to enforce the STC in the frozen state to be no less than the corresponding unfrozen value. The scaling exponent, $t$, characterizes the behavior of the STC near $\phi_c$, transitioning from the LCC-dominated end (i.e., $\lambda_{dry}$) to the HCC-dominated end (i.e., $\lambda_{sat}$). In this specific soil sample, the value of $t$ is smaller in frozen soil compared to unfrozen soil, while the larger $\theta_{ini}$ yields a smaller $t$ to reflect the shaper increase in STC.

**Table 2** Fitted values of model parameters and performance metrics of the unified model.

| Experiment | $\phi_c$ | $t$ | $\alpha$ | bias | RMSE | NSE |
|---|---|---|---|---|---|---|
| | ($m^3m^{-3}$) | | | ($Wm^{-1}°C^{-1}$) | ($Wm^{-1}°C^{-1}$) | |
| Unified unfrozen | 0.15 | 0.42 | 0.83 | 0.00 | 0.01 | 0.98 |
| Unified frozen ($\theta_{ini} = 0.20$) | 0.20 | 0.23 | 1.01 | 0.00 | 0.05 | 0.94 |
| Unified frozen ($\theta_{ini} = 0.24$) | 0.25 | 0.23 | 1.01 | −0.02 | 0.07 | 0.90 |
| Unified frozen ($\theta_{ini} = 0.27$) | 0.29 | 0.21 | 1.01 | −0.03 | 0.10 | 0.87 |
| Unified frozen ($\theta_{ini} = 0.30$) | 0.32 | 0.19 | 1.01 | −0.05 | 0.15 | 0.79 |

### 3.3 Established pedotransfer functions (PTFs)

PTFs find widespread use within LSMs to estimate the parameters of the STC model by leveraging more readily available soil properties, such as texture, porosity, and dry bulk density, as well as available state variables within LSMs such as soil temperature and moisture content. **Figure 5** illustrates the PTFs for the three parameters used in the unified model derived from the training dataset.

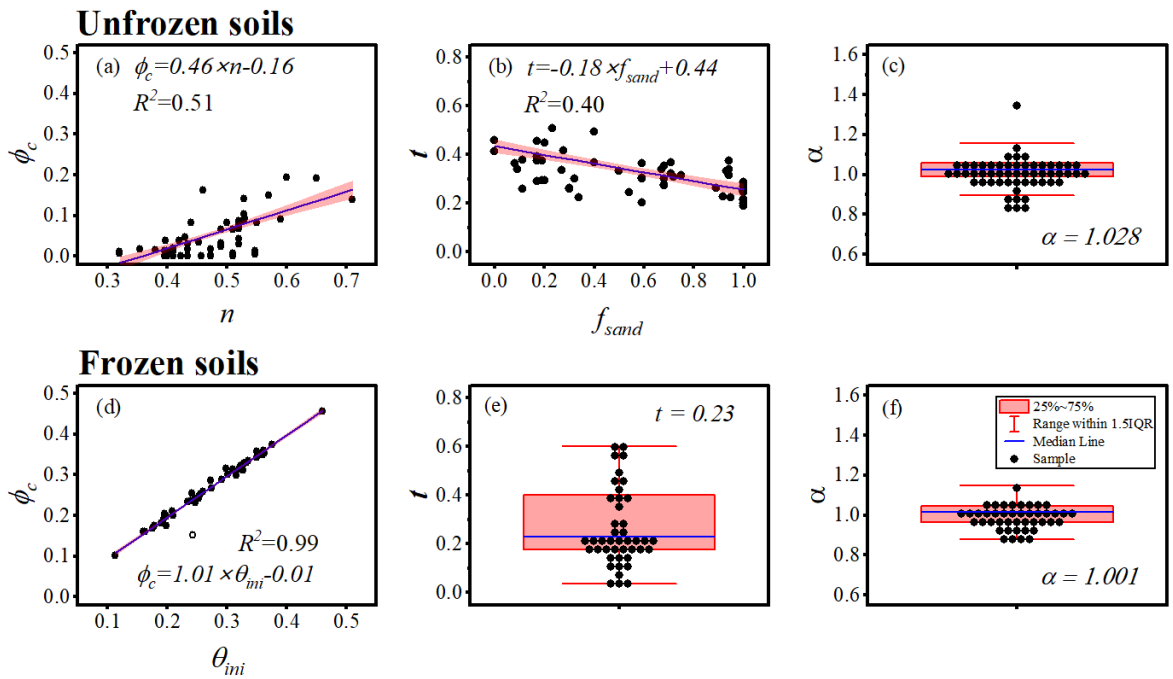


**Figure 5** Pedotransfer functions (PTFs) developed for the parameters: critical volume fraction ($\phi_c$), scaling exponent ($t$), and compensating factor ($\alpha$), leveraging basic soil properties for unfrozen (43 samples) (a–c) and frozen soils (55 samples) (d–f). The red shaded areas in (a, b, d) depict the 95% confidence band. The box plots (c, e, f) present the distributions of individual parameters where no significant correlation was identified with the basic soil properties, leading to the use of the median as the PTF. The boxes represent the range from the first to third quantile.

In unfrozen soils, the critical volume fraction ($\phi_c$) exhibits a positive correlation with porosity ($n$) (**Figure 5**a, Equation (26)). This diverges from the GD2016 model's approach that relies on clay content (Equation (2)). Both approaches, however, agree that soils with coarser textures typically entail smaller $\phi_c$. The divergence in the PTF for $\phi_c$ in the unified model might stem from the use of different training datasets. With a larger number of measurements (43 samples in this study, 17 in theirs), greater confidence can be placed in our results. For frozen soil, the physical meaning of

$\phi_c$ differs from that in unfrozen soils due to the involvement of phase change in the freezing process. Nevertheless, we observed a strong correlation with $\theta_{ini}$ with $R^2$ = 0.99 (**Figure 5**d, Equation (26)).

In contrast, predicting the scaling exponent $t$ presents challenges, as it is theoretically influenced by various factors such as soil texture and compaction. For unfrozen samples, this study employs sand content for estimation (**Figure 5**b and Equation (27)), differing from GD2016 which uses clay content (Equation (3)). However, for frozen samples, identifying significant functional relationships with basic soil properties proves elusive due to the limited availability of STC measurements. As an alternative, we provisionally adopt the median value (0.23) (**Figure 5**e, Equation (27)).

For the compensating factor ($\alpha$), a constant median value of 1.028 is adopted for unfrozen soils (**Figure 5**c, Equation (28)), and 1.001 for frozen soils (**Figure 5**f, Equation (28)). However, assigning constant values to $\alpha$ does not diminish the importance of including $\alpha$ in the model. As exemplified in Section 3.1, it assumes a vital role in facilitating accurate estimation of individual STC values. In addition, its proximity to 1 adds support to the plausibility of using the geometric mean method for STC calculations in saturated soils.

$$\phi_c = \begin{cases} 0.46 \times n - 0.16,\ R^2 = 0.51 & \text{unfrozen soils} \\ 1.01 \times \theta_{ini} - 0.01,\ R^2 = 0.99 & \text{frozen soils} \end{cases} \tag{26}$$

$$t = \begin{cases} -0.18 \times f_{sand} + 0.44,\ R^2 = 0.40 & \text{unfrozen soils} \\ 0.23 & \text{frozen soils} \end{cases} \tag{27}$$

$$\alpha = \begin{cases} 1.028 & \text{unfrozen soils} \\ 1.001 & \text{frozen soils} \end{cases} \tag{28}$$

### 3.4 Model performance using pedotransfer functions

Applying the respective PTFs, we assessed the performance of the unified model in comparison with the CK2005 and Tian2016 models using the testing dataset. Based on both quantitative metrics and visual comparison based on the 1:1 diagonal line, it becomes evident that the unified model outperforms the other two models (**Figure 6**).

For unfrozen soils, the testing dataset includes 40 samples with a total of 240 measurements. The predictions made by all three models largely fall within a 10% error margin. Both the unified model (bias = 0.01 $Wm^{-1}°C^{-1}$, RMSE = 0.12 $Wm^{-1}°C^{-1}$, NSE = 0.96) and the CK2005 model (bias = 0.03 $Wm^{-1}°C^{-1}$, RMSE = 0.15 $Wm^{-1}°C^{-1}$, NSE = 0.94) exhibit similar predictive skills, but show overestimations for soils with low thermal conductivities at low moisture content. On the other hand, the performance of Tian2016 deteriorates when dealing with measured thermal conductivities larger than 1.5 $Wm^{-1}°C^{-1}$, resulting in consistent underestimations for those high measured STCs (bias = 0.10 $Wm^{-1}°C^{-1}$, RMSE = 0.22 $Wm^{-1}°C^{-1}$, NSE = 0.86).

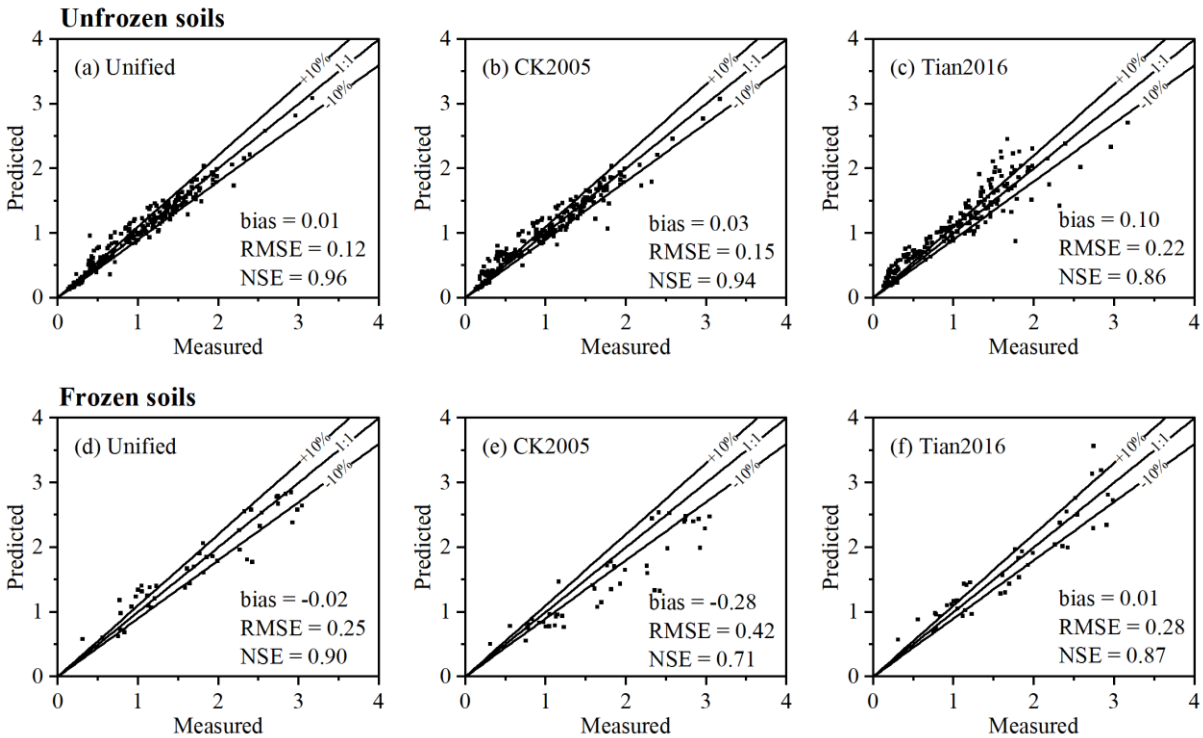


**Figure 6** Performance comparisons of the unified (a, d), CK2005 (b, e), and Tian2016 (c, f) models in predicting STC using respective PTFs based on independent testing datasets. The testing dataset comprises 40 samples with 240 measurements for unfrozen soils (a–c), and 38 samples with 65 measurements for frozen soils (d–f).

For frozen soils, the testing dataset is more limited, consisting of 38 samples with 65 measurements. Both the unified model (bias = −0.02 $Wm^{-1}°C^{-1}$, RMSE = 0.25 $Wm^{-1}°C^{-1}$, NSE = 0.90) and the Tian2016 model (bias = 0.01 $Wm^{-1}°C^{-1}$, RMSE = 0.28 $Wm^{-1}°C^{-1}$, NSE = 0.87) provide more accurate predictions compared to the CK2005 model (bias = −0.28 $Wm^{-1}°C^{-1}$, RMSE = 0.42 $Wm^{-1}°C^{-1}$, NSE = 0.71). Generally, the model performances in frozen soils are less satisfactory than in unfrozen soils, except for the Tian2016 model. However, it is important to note that this partly arises from the overlap between our testing dataset and the training dataset used to

develop the Tian2016 model, potentially inflating accuracy scores. Nevertheless, the unified model provides predictions that align more closely with the measurements, avoiding significant systematic underestimations observed in the CK2005 model (bias = −0.28 $Wm^{-1}°C^{-1}$).

# 4 Discussion

## 4.1 Unifying STC behaviors in frozen and unfrozen soils

The central focus of this study is the construction of a unified STC model capable of handling both unfrozen and frozen conditions. We extended upon the GD2016 model, which is developed exclusively for unfrozen soils. In unfrozen soil, the crucial factor influencing heat conduction is the emergence of "liquid capillary bridges" between particles characterized by $\phi_c$, which could significantly enhance the connectivity of heat conduction paths, leading to an increase in STC. Conversely, the rapid increase in STC during freezing primarily results from the replacement of liquid water with ice. The latter occupies a larger pore space and has higher thermal conductivity ($\lambda_{ice}$ = 2.22 $Wm^{-1}°C^{-1}$ versus $\lambda_{liq}$ = 0.56 $Wm^{-1}°C^{-1}$), thereby enhancing contacts among solid particles.

Despite these distinct mechanisms, the GEM framework allows the unification of these phenomena, with the saturated soil as the HCC (contingent on the thaw/freeze state) weighted by the volumetric total water content. The linkage between the two states is established through the liquid content before the onset of freezing ($\theta_{ini}$), which determines the maximal extent of liquid-to-ice conversion. The critical volume fraction ($\phi_c$) is thus well established as a function of $\theta_{ini}$ (Equation (26)).

### 4.2 Integration within GEM framework

McLachlan's development of the GEM equation (1987, 1986, 1985), integrating Bruggeman's symmetric/asymmetric theory and percolation theory, focused on artificially synthesized composite materials to derive the ranges of $\phi_c$ and $t$. However, the challenges in applying the original GEM equation to model soil transport properties, like STC, lie in the mixture of three phases (i.e., solid, liquid and gaseous states) and intricate structures involving shape, arrangement, and interaction of each component.

To address the gap between the GEM assumption of a bi-phase system and the complexity of multiple components in soil, we draw inspiration from the GD2016 model. Wetting and freezing processes are considered as water redistribution within pores, ignoring soil skeleton changes. The unified model focuses on pore fillers, designating air and water as the two bounds. Solid contribution is implicitly integrated into these bounds, designating dry soil as LCC and saturated soil as HCC. In this framework, the sum of fractions for LCC ($n - \theta_{liq} - \theta_{ice}$) and HCC ($\theta_{liq} + \theta_{ice}$) equals porosity ($n$), diverging from the original GEM equation where it equals 1. Alternative partitioning schemes, like air as LCC and saturated soil as HCC, were considered but proved limited in robustness.

Given the disparity between soil and artificially synthesized materials, parameters $\phi_c$ and $t$ may not align with previous studies, termed nonuniversal behavior. However, the rapid increase in STC during wetting and freezing aligns with percolation theory. Parameter $t$ characterizes conductivity change around $\phi_c$, depending on the ratio of thermal conductivities of HCC and LCC ($\lambda_{HCC}/\lambda_{LCC}$), structural and geometrical properties, and saturating fluids. Ghanbarian and Daigle et al. (2016) and our experiments (Section 3.2) both indicate that for materials with a small conductivity ratio ($\lambda_{HCC}/\lambda_{LCC} < 10^6$), $t$ decreases as the ratio decreases. Therefore, the applicable $t$ for modeling

STC ($\lambda_{HCC}/\lambda_{LCC} < 10^2$) takes a substantially small value (e.g., 0.225–0.369 for GD2016; 0.260–0.439 for the unified model). In materials with large $\lambda_{HCC}/\lambda_{LCC}$, $t$ decreases from 2 in an insulator-conductor system (Stauffer and Aharony, 1992) to 0.76 in a conductor-superconductor system (Bergman and Stroud, 1992) due to microstructural differences: one phase versus two phases forming a continuous heat pathway. For moist soil and partially frozen soil, where more components are involved, a smaller value of $t$ is expected.

Additionally, the contact angle between saturating fluid and solid matrix affects the continuous heat pathway, with a larger contact angle leading to a smaller $t$ (Ghanbarian et al., 2015; Ghanbarian and Daigle, 2016). Freezing processes result in a larger contact angle as substantiated experimentally (e.g., Wan et al., 2022). As a result, frozen soils show a further decrease in $t$ (a median of 0.23) compared to unfrozen soils (0.260–0.439), observed in specific soil samples (Section 3.3). Moreover, this study also notes that a larger $\theta_{ini}$ corresponds to a smaller $t$, which may be related to the synthesis impact of contact angle and microstructure.

### 4.3 Reevaluation of model performance

He et al. (2021a) recently reviewed 39 STC models for frozen soils using a dataset comprising 331 measurements. Their findings highlighted that a potential disparity between the claimed performance of these models and their real-world effectiveness as revealed through subsequent evaluation or testing. Among the tested models, the Becker et al. (1992) model emerged as the best for frozen soils, with a bias of −0.04 $Wm^{-1}°C^{-1}$, RMSE of 0.46 $Wm^{-1}°C^{-1}$ and NSE of 0.51. Meanwhile, Tian2016 excelled among theoretical models (bias = 0.19 $Wm^{-1}°C^{-1}$, RMSE = 0.51 $Wm^{-1}°C^{-1}$, NSE = 0.38).

In alignment with He et al. (2021a)'s methodology, we reevaluated the models involved in this study using all frozen soil datasets (74 samples with 255 measurements), without the separation of

training and testing datasets. Our dataset highly matched He et al. (2021a), with similar measurement sizes (255 in this study, 331 in theirs). Our evaluation indicated that the unified model's performance (bias = 0.11 $Wm^{-1}°C^{-1}$, RMSE = 0.43 $Wm^{-1}°C^{-1}$, NSE = 0.41) slightly surpassed that of Tian2016 (bias = 0.23 $Wm^{-1}°C^{-1}$, RMSE = 0.44 $Wm^{-1}°C^{-1}$, NSE = 0.38), which was already a top-performing model according to He et al. (2021a).

### 4.4 Challenges and limitations

Despite the advantages of uniformity, high accuracy as well as robustness, the proposed unified model still faces limitations that could impact its quality. Similar to most STC models for frozen soils, the model's accuracy partly relies on estimating unfrozen water content, often challenging to determine through cost-effective methods in the measurements (Tian et al., 2015; Zhou et al., 2014). This study estimated unfrozen water content using the matric potential equation (Equation (9)–(14)), a scheme with fully known parameters and widely used in prior STC modeling studies (He et al., 2021b; Tian et al., 2016). However, the relation between STC and freezing temperature (**Figure 3**) and the non-trivial underestimation during the early freezing stage (**Figure 4**) indicate room for improvement in unfrozen water content estimation (Hu et al., 2020; Lu et al., 2019). Furthermore, this flaw inevitably propagates to the calibrated parameters as well as the derived PTFs.

The calculation of solid thermal conductivity ($\lambda_{solid}$) can affect the unified model, as is common in other STC models. Ideally, it should be computed using the geometric mean method with typical mineralogical compositions (Côté and Konrad, 2005b). Practical simplifications often consider only two components: quartz ($\lambda_{quartz}$) and other minerals ($\lambda_{others}$). Given quartz's enrichment in coarse-grained particles and its often-missing content due to specialized equipment requirements (Calvet et al., 2016), half the sand content is used as an approximation. He et al. (2021a) evaluated

several methods for estimating quartz and endorsed this approach. In this study, a compensating factor α is therefore introduced for adjustment to account for potential biases.

Some discrepancies in the predictions made by the unified model could be attributed to the deviation of a uniform value of $t$ (0.23) from optimal values as demonstrated in the case of a silty clay loam example provided by Xu et al. (2020), where an optimized $t$ was close to 0.45. Currently, no strongly explanatory variable was found for $t$, necessitating future efforts to establish a reliable PTF for $t$. It should also be noted that the GD2016 model treats LCC and HCC ($\lambda_{dry}$ and $\lambda_{sat}$) as adjustable parameters, offering flexibility but reducing applicability when integrated into LSMs. The adjustment of $\lambda_{dry}$ and $\lambda_{sat}$ may lead to unrealistic bounds and shift essential model parameters ($\phi_c$ and $t$). Therefore, our unified model refrains from treating $\lambda_{dry}$ and $\lambda_{sat}$ as free parameters and we opt to directly estimate them from widely used empirical model (Equations (5)–(8)).

While the unified model currently demonstrated superior performance compared to other models, there is still a need for caution and further investigation. The connection between the model parameters and the intrinsic properties of soils, such as the fractal dimension of pore spaces and the distribution of grain sizes, demands more in-depth exploration.

# 5 Conclusions

Based on the GD2016 model for unfrozen soils, this study has presented a novel unified model capable of capturing the intricate STC behaviors of both unfrozen and frozen soils. The model, characterized by three key parameters (critical volume fraction, $\phi_c$; scaling exponent, $t$; and compensating factor, $\alpha$), treats dry soil as the low-conductivity component (weighted by air volume fraction) and saturated soil as the high-conductivity component (weighted by volumetric

liquid content in unfrozen states and by both liquid and ice fractions in frozen states). To facilitate integration into LSMs, pedotransfer functions for the model parameters were trained and evaluated using measurement data sourced from comprehensive literature. Two main conclusions were drawn:

(1) The unified model demonstrates notable strength in accurately reproducing the rapid increase in STC at low moisture conditions in unfrozen soils and the intricate STC dynamics throughout the complete freezing process. The critical parameter $\phi_c$ signifies the formation of "liquid capillary bridges" between solid particles during wetting processes and closely connects to the initial water content during freezing processes.

(2) The unified STC model, under rigorous comparison with established models CK2005 and Tian2016, consistently outperforms across various performance metrics. For unfrozen soils (40 samples, 240 measurements), it exhibits a bias of 0.01 $Wm^{-1}°C^{-1}$, RMSE of 0.12 $Wm^{-1}°C^{-1}$, and NSE of 0.96, while maintaining robust performance for frozen soils (38 samples, 65 measurements) with a bias of −0.02 $Wm^{-1}°C^{-1}$, RMSE of 0.25 $Wm^{-1}°C^{-1}$, and NSE of 0.90. These results affirm the superior predictive capability of the unified model over its counterparts, which is crucial for understanding and modeling ground temperature dynamics in cold regions.

**Acknowledgments**

The datasets used in this study were sourced from published literature, and the authors would like to extend their gratitude to those whose conducted the measurements. Special thanks are extended to Zhengchao Tian for sharing his dataset.

This work was supported by the National Natural Science Foundation of China (No. 42171125, 41931180) and the National Key Research and Development Program of China (No.

2022YFF0711703-02). Hailong Ji also received the support from the Postgraduate Research & Practice Innovation Program of Jiangsu Province (No. KYCX23_1695).

## CRediT authorship contribution statement

Z.N.: Conceptualization, Methodology, Resources, Writing – Original Draft, Writing – Review & Editing, Supervision, Funding acquisition; S. Z.: Conceptualization, Funding acquisition, Writing – Review & Editing; H. J.: Methodology, Software, Validation, Formal analysis, Investigation, Writing – Original Draft, Writing – Review & Editing; X. F.: Methodology, Investigation, Writing – Original Draft.

## Data Availability Statement

The associated data and simulation results of this study are publicly accessible through https://doi.org/10.6084/m9.figshare.23937303. The source codes for the unified model are available at https://doi.org/10.5281/zenodo.10279025. The optimization package v1.7.5 can be obtained from https://cran.r-project.org/package=pso.

## References

Anderson, D.M., Tice, A.R., 1972. Predicting unfrozen water contents in frozen soils from surface area measurements. Highw. Res. Rec. 393, 12–18.

Becker, B.R., Misra, A., Fricke, B.A., 1992. Development of correlations for soil thermal conductivity. Int. Commun. Heat Mass Transf. 19, 59–68. https://doi.org/10.1016/0735-1933(92)90064-O

Bergman, D.J., Stroud, D., 1992. Physical properties of macroscopically inhomogeneous media. Academic Press, pp. 147–269. https://doi.org/https://doi.org/10.1016/S0081-1947(08)60398-

7

Biskaborn, B.K., Smith, S.L., Noetzli, J., Matthes, H., Vieira, G., Streletskiy, D.A., Schoeneich, P., Romanovsky, V.E., Lewkowicz, A.G., Abramov, A., Allard, M., Boike, J., Cable, W.L., Christiansen, H.H., Delaloye, R., Diekmann, B., Drozdov, D., Etzelmüller, B., Grosse, G., Guglielmin, M., Ingeman-Nielsen, T., Isaksen, K., Ishikawa, M., Johansson, M., Johannsson, H., Joo, A., Kaverin, D., Kholodov, A., Konstantinov, P., Kröger, T., Lambiel, C., Lanckman, J.P., Luo, D., Malkova, G., Meiklejohn, I., Moskalenko, N., Oliva, M., Phillips, M., Ramos, M., Sannel, A.B.K., Sergeev, D., Seybold, C., Skryabin, P., Vasiliev, A., Wu, Q., Yoshikawa, K., Zheleznyak, M., Lantuit, H., 2019. Permafrost is warming at a global scale. Nat. Commun. 10. https://doi.org/10.1038/s41467-018-08240-4

Brooks, R.H., 1965. Hydraulic properties of porous media. Colorado State University.

Burke, E.J., Zhang, Y., Krinner, G., 2020. Evaluating permafrost physics in the Coupled Model Intercomparison Project 6 (CMIP6) models and their sensitivity to climate change. Cryosph. 14, 3155–3174. https://doi.org/10.5194/tc-14-3155-2020

Calvet, J.C., Fritz, N., Berne, C., Piguet, B., Maurel, W., Meurey, C., 2016. Deriving pedotransfer functions for soil quartz fraction in southern France from reverse modeling. SOIL 2, 615–629. https://doi.org/10.5194/soil-2-615-2016

Campbell, G.S., Jungbauer Jr, J.D., Bidlake, W.R., Hungerford, R.D., 1994. Predicting the effect of temperature on soil thermal conductivity. Soil Sci. 158, 307–313.

Chen, S.X., 2008. Thermal conductivity of sands. Heat Mass Transf. 44, 1241–1246. https://doi.org/10.1007/s00231-007-0357-1

Claus, B., 2022. pso: Particle Swarm Optimization.

Colombo, N., Salerno, F., Gruber, S., Freppaz, M., Williams, M., Fratianni, S., Giardino, M., 2018.

Review: Impacts of permafrost degradation on inorganic chemistry of surface fresh water. Glob. Planet. Change 162, 69–83. https://doi.org/10.1016/j.gloplacha.2017.11.017

Côté, J., Konrad, J.-M., 2005a. A generalized thermal conductivity model for soils and construction materials. Can. Geotech. J. 42, 443–458. https://doi.org/10.1139/t04-106

Côté, J., Konrad, J.-M., 2005b. Thermal conductivity of base-course materials. Can. Geotech. J. 42, 61–78. https://doi.org/10.1139/t04-081

Dai, Y.J., Wei, N., Yuan, H., Zhang, S.P., Wei, S.G., Liu, S.F., Lu, X.J., Xin, Y.F., 2019. Evaluation of soil thermal conductivity schemes for use in land surface modeling. J. Adv. Model. Earth Syst. 11, 3454–3473. https://doi.org/10.1029/2019ms001723

Dai, Y.J., Zeng, X.B., Dickinson, R.E., Baker, I., Bonan, G.B., Bosilovich, M.G., Denning, A.S., Dirmeyer, P.A., Houser, P.R., Niu, G.Y., Oleson, K.W., Schlosser, C.A., Yang, Z.L., 2003. The Common Land Model. Bull. Am. Meteorol. Soc. 84, 1013–1023. https://doi.org/10.1175/BAMS-84-8-1013

De Vries, D.A., 1963. Thermal properties of soils, in: Van Dijk, W.R. (Ed.), Physics of Plant Environment. North-Holland Publishing Corporation, Amsterdam, pp. 210–235.

Ding, Y., Mu, C., Wu, T., Hu, G., Zou, D., Wang, D., Li, W., Wu, X., 2021. Increasing cryospheric hazards in a warming climate. Earth-Science Rev. 213, 103500. https://doi.org/10.1016/j.earscirev.2020.103500

Dong, Y., McCartney, J.S., Lu, N., 2015. Critical review of thermal conductivity models for unsaturated soils 33, 207–221. https://doi.org/10.1007/s10706-015-9843-2

Du, Y., Li, R., Zhao, L., Yang, C., Wu, T., Hu, G., Xiao, Y., Zhu, X., Yang, S., Ni, J., Ma, J., 2020. Evaluation of 11 soil thermal conductivity schemes for the permafrost region of the central Qinghai-Tibet Plateau. CATENA 193, 104608.

https://doi.org/https://doi.org/10.1016/j.catena.2020.104608

Farouki, O.T., 1982. Evaluation of methods for calculating soil thermal conductivity. US Army Corps of Engineers, Cold Regions Research & Engineering Laboratory.

Farouki, O.T., 1981. Thermal Properties of Soils.

Ghanbarian, B., Daigle, H., 2016. Thermal conductivity in porous media: Percolation-based effective-medium approximation. Water Resour. Res. 52, 295–314. https://doi.org/10.1002/2015WR017236

Ghanbarian, B., Daigle, H., Hunt, A.G., Ewing, R.P., Sahimi, M., 2015. Gas and solute diffusion in partially saturated porous media: Percolation theory and Effective Medium Approximation compared with lattice Boltzmann simulations. J. Geophys. Res. Solid Earth 120, 182–190. https://doi.org/https://doi.org/10.1002/2014JB011645

Harp, D.R., Atchley, A.L., Painter, S.L., Coon, E.T., Wilson, C.J., Romanovsky, V.E., Rowland, J.C., 2016. Effect of soil property uncertainties on permafrost thaw projections: a calibration-constrained analysis. Cryosph. 10, 341–358. https://doi.org/10.5194/tc-10-341-2016

He, H., Flerchinger, G.N., Kojima, Y., Dyck, M., Lv, J., 2021a. A review and evaluation of 39 thermal conductivity models for frozen soils. Geoderma 382, 114694. https://doi.org/10.1016/j.geoderma.2020.114694

He, H., Flerchinger, G.N., Kojima, Y., He, D., Hardegree, S.P., Dyck, M.F., Horton, R., Wu, Q., Si, B., Lv, J., Wang, J., 2021b. Evaluation of 14 frozen soil thermal conductivity models with observations and SHAW model simulations. Geoderma 403, 115207. https://doi.org/10.1016/j.geoderma.2021.115207

Horai, K., 1971. Thermal conductivity of rock-forming minerals. J. Geophys. Res. 76, 1278–1308. https://doi.org/10.1029/JB076i005p01278

Hu, G., Zhao, L., Zhu, X., Wu, X., Wu, T., Li, R., Xie, C., Hao, J., 2020. Review of algorithms and parameterizations to determine unfrozen water content in frozen soil. Geoderma 368, 114277. https://doi.org/https://doi.org/10.1016/j.geoderma.2020.114277

Hu, J., Nan, Z., Ji, H., 2022. Spatiotemporal characteristics of NPP changes in frozen ground areas of the Three-River Headwaters region, China: A regional modeling perspective. Front. Earth Sci. 10, 178. https://doi.org/10.3389/feart.2022.838558

Johansen, O., 1975. Thermal Conductivity of Soils. University of Trondheim, Norway.

Kasubuchi, T., Momose, T., Tsuchiya, F., Tarnawski, V., 2007. Normalized thermal conductivity model for three Japanese soils. Trans. Japanese Soc. Irrig. 251, 529–533.

Kersten, M.S., 1949. Thermal properties of soils. University of Minnesota, Minneapolis, MN.

Kirkpatrick, S., 1973. Percolation and conduction. Rev. Mod. Phys. 45, 574–588. https://doi.org/10.1103/RevModPhys.45.574

Kojima, Y., Heitman, J.L., Noborio, K., Ren, T., Horton, R., 2018. Sensitivity analysis of temperature changes for determining thermal properties of partially frozen soil with a dual probe heat pulse sensor. Cold Reg. Sci. Technol. 151, 188–195. https://doi.org/10.1016/j.coldregions.2018.03.022

Koven, C.D., Riley, W.J., Stern, A., 2013. Analysis of permafrost thermal dynamics and response to climate change in the CMIP5 Earth System Models. J. Clim. 26, 1877–1900. https://doi.org/https://doi.org/10.1175/JCLI-D-12-00228.1

Kurylyk, B.L., Watanabe, K., 2013. The mathematical representation of freezing and thawing processes in variably-saturated, non-deformable soils. Adv. Water Resour. 60, 160–177. https://doi.org/10.1016/j.advwatres.2013.07.016

Li, R., Zhao, L., Wu, T., Wang, Q., Ding, Y., Yao, J., Wu, X., Hu, G., Xiao, Y., Du, Y., Zhu, X.,

Qin, Y., Yang, S., Bai, R., Du, E., Liu, G., Zou, D., Qiao, Y., Shi, J., 2019. Soil thermal conductivity and its influencing factors at the Tanggula permafrost region on the Qinghai–Tibet Plateau. Agric. For. Meteorol. 264, 235–246. https://doi.org/https://doi.org/10.1016/j.agrformet.2018.10.011

Lu, J., Pei, W., Zhang, X., Bi, J., Zhao, T., 2019. Evaluation of calculation models for the unfrozen water content of freezing soils. J. Hydrol. 575, 976–985. https://doi.org/https://doi.org/10.1016/j.jhydrol.2019.05.031

Lu, N., Dong, Y., 2015. Closed-form equation for thermal conductivity of unsaturated soils at room temperature. J. Geotech. Geoenvironmental Eng. 141, 4015016. https://doi.org/10.1061/(ASCE)GT.1943-5606.0001295

Lu, S., Ren, T., Gong, Y., Horton, R., 2007. An improved model for predicting soil thermal conductivity from water content at room temperature. Soil Sci. Soc. Am. J. 71, 8–14. https://doi.org/10.2136/sssaj2006.0041

Lu, Y., Lu, S., Horton, R., Ren, T., 2014. An empirical model for estimating soil thermal conductivity from texture, water content, and bulk density. Soil Sci. Soc. Am. J. 78, 1859–1868. https://doi.org/10.2136/sssaj2014.05.0218

Lu, Y., Yu, W., Hu, D., Liu, W., 2018. Experimental study on the thermal conductivity of aeolian sand from the Tibetan Plateau. Cold Reg. Sci. Technol. 146, 1–8. https://doi.org/10.1016/j.coldregions.2017.11.006

McInnes, K., 1981. Thermal conductivities of soils from dryland wheat regions in Eastern Washington. Washington State University, WA, USA.

McLachlan, D.S., 1987. An equation for the conductivity of binary mixtures with anisotropic grain structures. J. Phys. C Solid State Phys. 20, 865–877. https://doi.org/10.1088/0022-

3719/20/7/004

McLachlan, D.S., 1986. Equations for the conductivity of macroscopic mixtures. J. Phys. C Solid State Phys. 19, 1339–1354. https://doi.org/10.1088/0022-3719/19/9/007

McLachlan, D.S., 1985. Equation for the conductivity of metal-insulator mixtures. J. Phys. C Solid State Phys. 18, 1891–1897. https://doi.org/10.1088/0022-3719/18/9/022

McLachlan, D.S., Blaszkiewicz, M., Newnham, R.E., 1990. Electrical resistivity of composites. J. Am. Ceram. Soc. 73, 2187–2203. https://doi.org/10.1111/j.1151-2916.1990.tb07576.x

Niu, G.Y., Yang, Z.L., Mitchell, K.E., Chen, F., Ek, M.B., Barlage, M., Kumar, A., Manning, K., Niyogi, D., Rosero, E., Tewari, M., Xia, Y., 2011. The community Noah land surface model with multiparameterization options (Noah-MP): 1. Model description and evaluation with local-scale measurements. J. Geophys. Res. Atmos. 116, 12109. https://doi.org/10.1029/2010JD015139

Overduin, P.P., Kane, D.L., van Loon, W.K.P., 2006. Measuring thermal conductivity in freezing and thawing soil using the soil temperature response to heating. Cold Reg. Sci. Technol. 45, 8–22. https://doi.org/10.1016/j.coldregions.2005.12.003

Penner, E., Johnston, G.H., Goodrich, L.E., 1975. Thermal conductivity laboratory studies of some Mackenzie Highway soils. Can. Geotech. J. 12, 271–288. https://doi.org/10.1139/t75-033

Peters-Lidard, C.D., Blackburn, E., Liang, X., Wood, E.F., 1998. The effect of soil thermal conductivity parameterization on surface energy fluxes and temperatures. J. Atmos. Sci. 55, 1209–1224. https://doi.org/10.1175/1520-0469(1998)055<1209:TEOSTC>2.0.CO;2

Ren, Y., Yue, P., Zhang, Q., Wang, J., Yang, J., Lu, Y., Fu, Z., 2023. Effects of soil thermal conductivity on rainy season precipitation in northern China. J. Hydrometeorol. 24, 73–86. https://doi.org/10.1175/JHM-D-22-0003.1

Sadeghi, M., Ghanbarian, B., Horton, R., 2018. Derivation of an explicit form of the percolation-based effective-medium approximation for thermal conductivity of partially saturated soils. Water Resour. Res. 54, 1389–1399. https://doi.org/10.1002/2017WR021714

Saxton, K.E., Rawls, W.J., Romberger, J.S., Papendick, R.I., 1986. Estimating generalized soil-water characteristics from texture. Soil Sci. Soc. Am. J. 50, 1031–1036. https://doi.org/10.2136/sssaj1986.03615995005000040039x

Smith, S.L., O'Neill, H.B., Isaksen, K., Noetzli, J., Romanovsky, V.E., 2022. The changing thermal state of permafrost. Nat. Rev. Earth Environ. 3, 10–23. https://doi.org/10.1038/s43017-021-00240-1

Smits, K.M., Sakaki, T., Limsuwat, A., Illangasekare, T.H., 2010. Thermal conductivity of sands under varying moisture and porosity in drainage–wetting cycles. Vadose Zo. J. 9, 172–180. https://doi.org/10.2136/vzj2009.0095

Stauffer, D., Aharony, A., 1992. Introduction To Percolation Theory, 2nd ed. Taylor & Francis, London, U.K. https://doi.org/https://doi.org/10.1201/9781315274386

Sun, J., Yang, K., Lu, H., Zhou, X., Li, X., Chen, Y., Guo, W., Wright, J.S., 2023. Land–atmosphere feedbacks weaken the cooling effect of soil organic matter property toward deep soil on the eastern Tibetan Plateau. J. Hydrometeorol. 24, 105–117. https://doi.org/10.1175/JHM-D-22-0074.1

Tarnawski, V.R., Leong, W.H., 2012. A series-parallel model for estimating the thermal conductivity of unsaturated soils. Int. J. Thermophys. 33, 1191–1218. https://doi.org/10.1007/s10765-012-1282-1

Tarnawski, V.R., Momose, T., McCombie, M.L., Leong, W.H., 2015. Canadian field soils III. thermal-conductivity data and modeling. Int. J. Thermophys. 36, 119–156.

https://doi.org/10.1007/s10765-014-1793-z

Tian, Z., Heitman, J., Horton, R., Ren, T., 2015. Determining soil ice contents during freezing and thawing with Thermo-Time Domain reflectometry. Vadose Zo. J. 14. https://doi.org/10.2136/vzj2014.12.0179

Tian, Z., Lu, Y., Horton, R., Ren, T., 2016. A simplified de Vries-based model to estimate thermal conductivity of unfrozen and frozen soil. Eur. J. Soil Sci. 67, 564–572. https://doi.org/10.1111/ejss.12366

Wan, X., Pei, W., Lu, J., Qiu, E., Yan, Z., Pirhadi, N., Zhu, J., 2022. Analytical model to predict unfrozen water content based on the probability of ice formation in soils. Permafr. Periglac. Process. 33, 436–451. https://doi.org/10.1002/ppp.2167

Wang, J., He, H., Li, M., Dyck, M., Si, B., Lv, J., 2021. A review and evaluation of thermal conductivity models of saturated soils. Arch. Agron. Soil Sci. 67, 974–986. https://doi.org/10.1080/03650340.2020.1771315

Wang, Y., Xiao, J., Ma, Y., Ding, J., Chen, X., Ding, Z., Luo, Y., 2023. Persistent and enhanced carbon sequestration capacity of alpine grasslands on Earth's Third Pole. Sci. Adv. 9, eade6875. https://doi.org/10.1126/sciadv.ade6875

Wu, X., Nan, Z., Zhao, S., Zhao, L., Cheng, G., 2018. Spatial modeling of permafrost distribution and properties on the Qinghai-Tibet Plateau. Permafr. Periglac. Process. 29, 86–99. https://doi.org/10.1002/PPP.1971

Xu, X., Zhang, W., Fan, C., Li, G., 2020. Effects of temperature, dry density and water content on the thermal conductivity of Genhe silty clay. Results Phys. 16, 102830. https://doi.org/10.1016/j.rinp.2019.102830

Zhang, G., Nan, Z., Hu, N., Yin, Z., Zhao, L., Cheng, G., Mu, C., 2022. Qinghai-Tibet Plateau

Permafrost at risk in the late 21st century. Earth's Futur. 10, e2022EF002652. https://doi.org/10.1029/2022EF002652

Zhang, M., Lu, J., Lai, Y., Zhang, X., 2018. Variation of the thermal conductivity of a silty clay during a freezing-thawing process. Int. J. Heat Mass Transf. 124, 1059–1067. https://doi.org/10.1016/j.ijheatmasstransfer.2018.02.118

Zhang, N., Wang, Z., 2017. Review of soil thermal conductivity and predictive models. Int. J. Therm. Sci. 117, 172–183. https://doi.org/10.1016/j.ijthermalsci.2017.03.013

Zhao, L., Wu, Q., Marchenko, S.S., Sharkhuu, N., 2010. Thermal state of permafrost and active layer in Central Asia during the international polar year. Permafr. Periglac. Process. 21, 198–207. https://doi.org/10.1002/ppp.688

Zhao, Y., Nan, Z., Ji, H., Zhao, L., 2022. Convective heat transfer of spring meltwater accelerates active layer phase change in Tibet permafrost areas. Cryosphere 16, 825–849. https://doi.org/10.5194/TC-16-825-2022

Zhou, X., Zhou, J., Kinzelbach, W., Stauffer, F., 2014. Simultaneous measurement of unfrozen water content and ice content in frozen soil using gamma ray attenuation and TDR. Water Resour. Res. 50, 9630–9655. https://doi.org/10.1002/2014WR015640